β1-subunit–induced structural rearrangements of the Ca^{2+}- and voltage-activated K^+ (BK) channel

Juan P. Castillo[a,b,1], Jorge E. Sánchez-Rodríguez[c,d,1], H. Clark Hyde[c,1], Cristian A. Zaelzer[a], Daniel Aguayo[a,e], Romina V. Sepúlveda[e], Louis Y. P. Luk[f], Stephen B. H. Kent[c,f], Fernando D. Gonzalez-Nilo[a,e], Francisco Bezanilla[a,c,2], and Ramón Latorre[a,2]

[a]Centro Interdisciplinario de Neurociencias de Valparaíso, Facultad de Ciencias, Universidad de Valparaíso, Valparaiso 2360103, Chile; [b]Departamento de Biologia, Facultad de Ciencias, Universidad de Chile, Santiago 7800003, Chile; [c]Department of Biochemistry and Molecular Biology, University of Chicago, Chicago, IL 60637; [d]Departamento de Física, Universidad de Guadalajara, Guadalajara, Jalisco, 44430, Mexico; [e]Universidad Andrés Bello, Center for Bioinformatics and Integrative Biology, Facultad de Ciencias Biológicas, Santiago 8370146, Chile; and [f]Department of Chemistry, University of Chicago, Chicago, IL 60637

Large-conductance Ca^{2+}- and voltage-activated K^+ (BK) channels are involved in a large variety of physiological processes. Regulatory β-subunits are one of the mechanisms responsible for creating BK channel diversity fundamental to the adequate function of many tissues. However, little is known about the structure of its voltage sensor domain. Here, we present the external architectural details of BK channels using lanthanide-based resonance energy transfer (LRET). We used a genetically encoded lanthanide-binding tag (LBT) to bind terbium as a LRET donor and a fluorophore-labeled iberiotoxin as the LRET acceptor for measurements of distances within the BK channel structure in a living cell. By introducing LBTs in the extracellular region of the α- or β1-subunit, we determined (i) a basic extracellular map of the BK channel, (ii) β1-subunit–induced rearrangements of the volt-age sensor in α-subunits, and (iii) the relative position of the β1-sub-unit within the α/β1-subunit complex.

lanthanide resonance energy transfer | BK channels | β1-subunit

Important physiological processes involve Ca^{2+} entry into cells mediated by voltage-dependent Ca^{2+} channels. This divalent cation influx is essential for life because it permits, for example, the adequate functioning of smooth muscle or neurosecretion to occur. Some mechanism must be put into action, however, to control Ca^{2+} influx, either to dampen or to stop the physiological effects of the cytoplasmic increase in Ca^{2+}. In many cases, this dampening mechanism is accomplished by one of the most broadly expressed channels in mammals: the large-conductance Ca^{2+}- and voltage-activated K^+ (BK) channel (1–3). Because there is a single gene coding for the BK channel (Slowpoke KNCMA1), channel diversity must be a consequence of alternative splicing and/or interaction with regulatory subunits. In fact, both mechanisms account for BK channel diversity, but the most dramatic changes in BK channel properties are brought about through the interaction with regulatory subunits, membrane-integral proteins, denominated BK β-subunits (β1–β4) (4–7) and the recently discovered γ-subunits (γ1–γ4) (8, 9).

Structurally, the BK channel is a homotetramer of its pore-forming α-subunit and is a member of the voltage-dependent po-tassium (Kv) channel family. Distinct from Kv channels, however, BK channel subunits are composed of seven transmembrane do-mains S0–S6 (10, 11). Little is known about the detailed structure of the membrane-spanning portion of the BK channel, or of the α/β1-subunit complex. Here, we used a variant of Förster resonance energy transfer (FRET), called lanthanide-based resonance energy transfer (LRET), to determine the positions of the N terminus (NT) and S0, S1, and S2 transmembrane segments of the α-subunit of the BK channel, as well as the position of the β1-subunit in the α/β1-subunit complex. LRET uses luminescent lanthanides (e.g., Tb^{3+}) as donor instead of conventional fluorophores. This technique has been successfully used to measure intramolecular distances and to track voltage-dependent structural changes in voltage-dependent K^+ and Na^+ channels (12–16). The advantages of this technique over FRET have been discussed in detail elsewhere (17), and only its highlights will be given here. Briefly, the isotropic emission of Tb^{3+} ensures that the maximum error in distance estimation due to the orientation factor (κ^2) does not exceed ±10% in the range of 10–120 Å (17). Because Tb^{3+} has a spiked emission spectrum, it is possible to isolate the sensitized emission (SE) of the acceptor with relative ease by using an adequate optical filter. Additionally, we used the genetically encoded lanthanide-binding tag (LBT) to chelate Tb^{3+} donor within the protein structure (18) (Fig. 1A). Because the LBT-Tb^{3+} emission decay has a well-defined time constant of ∼2.4 ms, the donor-only (DO) emission (i.e., the donor emission in the absence of the acceptor) is very specific and distinguishable from background (13, 18, 19). Also, because the LBT is incorporated into the backbone of the protein, the donor becomes tied to the structure of the channel, likely decreasing the uncertainty of the donor position. Any distortion of the LBT structure that modifies Tb^{3+} accessibility to water will decrease its decay time constant. Therefore, by measuring the Tb^{3+} decay, it is possible to infer whether the LBT remains intact in the final structure. More-over, the crystal structure of the LBT has been determined (18), making it possible to perform molecular dynamics (MD) simulations of the LBT-BK chimeric channels using homology-based models. The flexibility of the LBT–Tb^{3+} complex would place the Tb^{3+} atom at 5–8 Å from the LBT insertion site, giving us a concise

Significance

Large-conductance Ca^{2+}- and voltage-activated K^+ (BK) channels play many physiological roles, ranging from the maintenance of smooth muscle tone to the modulation of alcohol tolerance. In most cases, this physiological versatility of the BK channel is due to the association of the pore-forming α-subunit with β-subunits. Therefore, it is of importance to know what the structural con-sequences of this association are. Here, using lanthanide-based resonance energy transfer, we were able to determine the ex-tracellular position of transmembrane segments S0–S2 with and without the β1-subunit and the position of the two trans-membrane segments of the β1 subunit in the α/β1-subunit com-plex. We concluded that β1 produces rearrangements of the BK voltage sensor domain.

Author contributions: J.P.C., J.E.S.-R., H.C.H., D.A., R.V.S., F.D.G.-N., F.B., and R.L. designed research; J.P.C., J.E.S.-R., H.C.H., and C.A.Z. performed research; H.C.H., L.Y.P.L., S.B.H.K., and F.B. contributed new reagents/analytic tools; J.P.C., J.E.S.-R., H.C.H., C.A.Z., D.A., R.V.S., F.D.G.-N., F.B., and R.L. analyzed data; and J.P.C., H.C.H., F.B., and R.L. wrote the paper.

Reviewers: C.J.L., Washington University School of Medicine; and R.O., University of California, Los Angeles.

The authors declare no conflict of interest.

[1]J.P.C., J.E.S.-R., and H.C.H. contributed equally to this work.

[2]To whom correspondence may be addressed. Email: fbezanilla@uchicago.edu or ramon.latorre@uv.cl.

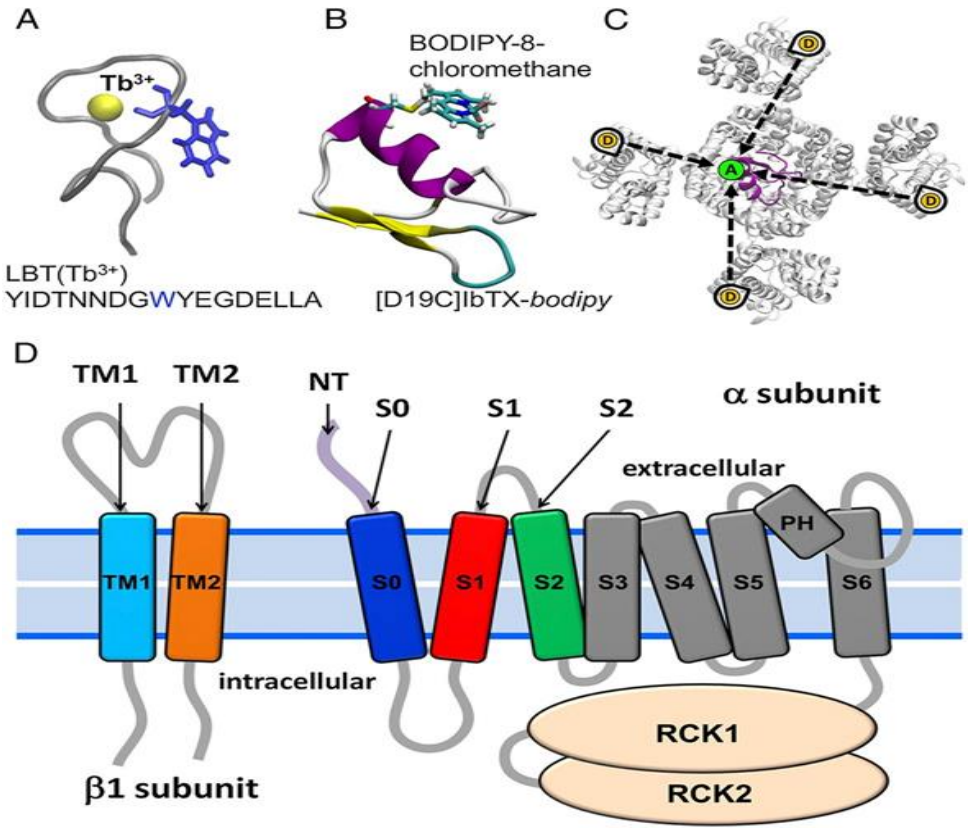

Fig. 1. LRET strategy in the BK channel. (A) LBT binds a luminescent Tb^{3+} ion with high affinity, acting as a LRET donor. Highlighted in blue is the tryptophan, which serves as an antenna that sensitizes Tb^{3+} to become excited by a 266-nm laser pulse. (B) Fluorescent probe bodipy interacts via LRET with the LBT-chelated Tb^{3+} with an R_0 value of 39.7 Å. The bodipy molecule is covalently conjugated to IbTX at position D19C. (C) Due to the homotetrameric symmetry of the BK channel, each of the four donors (D) can transfer energy via LRET to the single acceptor (A) that is offset from the pore axis (dotted black arrows). The four different distances result in multiexponential decay of SE. (D) LBT constructs were engineered (one LBT at a time) within the BK α-subunit: NT; on the extracellular side of transmembrane segments S0, S1, and S2; and within the BK β1-subunit on the extracellular side of transmembrane segments TM1 and TM2. RCK, Regulator of Conductance of K+.

picture of the general architecture of the external aspect of the BK channel (13).

As a reference site to locate the acceptor, we used the successful approach of labeling BK with a specific pore-blocking toxin, the scorpion toxin iberiotoxin (IbTX), which binds to the external as-pect of the BK pore with high affinity (13–15, 20, 21). One of the advantages of this approach is that the relative position of the acceptor can be modeled because the structure of a related toxin, charybdotoxin (CTX), in complex with the Kv1.2/2.1 paddle chi-mera has been determined (22). Because the BK channels are tetramers organized in an axial fourfold symmetry around the K^+ selective pore, the location of the toxin, and hence the location of the acceptor fluorophore, can be modeled. We synthesized IbTX in solid phase with a modified cysteine at residue 19 and labeled with BODIPY-8-chloromethane (referred to as bodipy throughout this paper) as a fluorescent probe. The short linker of bodipy reduces uncertainty in the acceptor position (Fig. 1B). The labeled toxin was then used as an acceptor for the Tb^{3+} donor emission.

We used a methodology of analysis capable of extracting the position of the four donors from the SE of the acceptor, taking advantage of the fourfold symmetry of K^+ channels (Fig. 1C). This method has been successfully tested in Shaker K^+ channels (13). By changing the position of the LBT motif to different residues of the channel, we constructed a map of the extracellular arrangement of the S0, S1, and S2 segments, as well as the position of the NT of the BK channel, in the absence and presence of the auxiliary β1-sub-unit. In addition, by introducing the LBT in different positions of the β1-subunit, we located this subunit with respect to the α-subunit.

Results

LRET in LBT-Containing BK Channels. We selected LBT insertion sites within the BK α- and β1-subunits to estimate the location of the voltage sensor domain (VSD) with respect to the channel's pore (i) in the absence of the regulatory β1-subunit and (ii) after coexpressing the BK α/β1-complex. Fig. 1D shows four insertion sites in the BK α-subunit that are in the extracellular face of the protein: NT (D15-LBT-S16), S0 (W22-LBT-W23), S1 (S134-LBT-S135), and S2 (D147-LBT-F148). Fig. 1D also shows insertion sites in the β1-subunit. They are located near the C terminus of trans-membrane segment TM1 (L41-LBT-Y42) and near the NT of TM2 (R150-LBT-L151). All these constructs were expressed in the membrane of Xenopus laevis oocytes and tested with electrophys-iological methods to confirm that they still operate as BK channels. No major alterations were observed after introduction of the LBT motif to any α-LBT constructs reported here (Fig. S1), suggesting that insertion of the LBT motif did not change the structure of the protein. The effect of the β1-subunit was also assessed with α-LBT

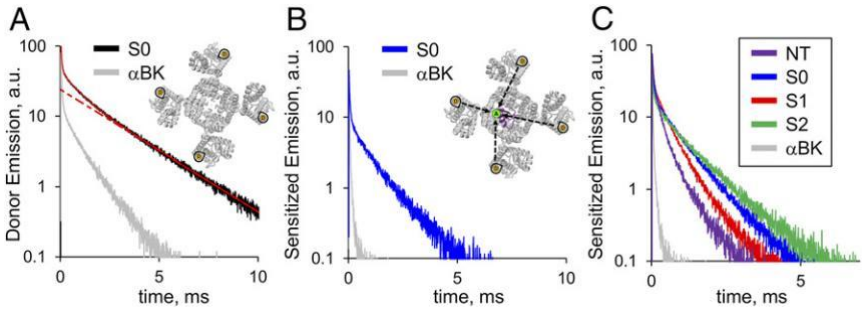

Fig. 2. LRET measurements of LBT-tagged BK constructs. (A) Representative DO emission recording from an oocyte expressing the S0 construct. The red solid line represents a three-exponential fit. The slowest component with a time constant of ≈2.5 ms (red dotted line) corresponds to the decay from Tb^{3+} bound to LBT (Inset). (B) SE of the acceptor recorded after addition of IbTX-bodipy from the same oocyte of A. (Inset) Attached fluorophore acts as an LRET acceptor. Gray traces in A and B correspond to DO and SE control experiments, respectively, using WT BK α-subunit (α-BK). (C) Representative SE recorded from NT, S0, S1, and S2 constructs exhibited characteristic decay kinetics. Because there are four donors and one acceptor per channel, SE decays are composed of four energy transfer-based exponential components. Faster SE kinetics indicate that the four donors are positioned in closer proximity to the acceptor. a.u., arbitrary units.

constructs, as well as for TM1 and TM2 constructs coexpressed with wild-type (WT) α-BK subunit to confirm that they maintain the α/β1-BK phenotype (Fig. S2). In addition, several LBT insertion sites were designed and tested in the very short linker region between S3 and S4 of αBK. Although these constructs produced robust macroscopic currents, donor emission signal was absent, likely because of a defective LBT-Tb^{3+} structure.

All LRET experiments described below were performed hold-ing the membrane potential at −80 mV to ensure that all channels were closed with their voltage sensors in the resting state. LRET experiments at depolarizing voltages large enough to open the channels fully were not possible due to the high expression of the LBT-BK chimeras that precluded adequate voltage control of the oocytes at such high potentials.

We tested the DO signal from all LBT-BK constructs by exciting the sample with a short laser pulse (5 ns) at 266 nm and obtained robust luminescence decays in all cases. Fig. 2A shows the time-resolved donor emission decay from an oocyte expressing the S0 construct. The slowest component of the decay has a time constant $\tau_D \sim 2.4$ ms [rate constant $(k_D) \sim 417\ s^{-1}$], which is absent in oocytes expressing WT BK channel (Fig. 2A, gray trace). This component is the expected decay of Tb^{3+} bound to LBT in the absence of acceptor (Fig. 2A, Inset). Our results show that all LBTs inserted in the α-subunit, as well as the β1-subunit, produced DO decay times greater than 2.15 ms, indicating that the LBT struc-ture is maintained after insertion into either protein (Table S1).

When 500 nM IbTX-bodipy is added to the bath solution, the excited donors (LBT-Tb^{3+}) transfer energy by long-range dipole-dipole resonance to the attached fluorophore near the pore of the channel (Fig. 2B, Inset). Because the acceptor, bodipy, is fluorescent, it is possible to measure the SE, defined as the emission of acceptors excited only through energy transfer from donors. In LRET, the lifetime of the SE decay gives a direct measurement of the excited donor lifetime in the presence of acceptor, because the intrinsic acceptor lifetime is in the nanosecond scale, whereas the excited donor lifetime is in the millisecond scale (17, 23). We used a bandpass optical filter to isolate the SE of bodipy (Fig. 2B, blue trace) that effectively blocks any contamination from the donor emission. Because the acceptor is not located on the symmetry axis of the channel (Fig. 1C), there is more than one donor–acceptor distance, resulting in multiexponential SE decay (13–15). A com-parison between the kinetics of SE traces from different constructs (Fig. 2C) reveals that the relative position of the donor relative to the static acceptor (offset from the pore axis) differs among constructs.

Dramatic effects are observed in the SE decay kinetics from different constructs when they are coexpressed with the β1-subunit. The effect of the β1-subunit is different for each of the four α-LBT constructs tested above. In the case of NT, β1 greatly slowed the SE kinetics (Fig. 3A). On the other hand, we observed less dramatic changes in the SE kinetics of S0, S1, and S2 (Fig. 3 B–D). These results suggest that the α/β1 interaction promotes a change in the architecture of the VSD of the BK channel.

As was done for the α-subunit, two LBT constructs of the β1-subunit were engineered with insertion sites near the extracel-lular side of the TM1 and TM2 segments (Fig. 1D). These constructs showed SE with characteristic kinetics indicating their different locations relative to the channel structure (Fig. 3E).

A Spatial Map of the Extracellular Face of the BK Channel. To retrieve quantitative information from the SE recordings, we used the symmetrical nanopositioning system (SNPS) to generate a spatial map of the different donor positions (13). This methodology as-sumes a pyramid-like geometric model, which considers that the

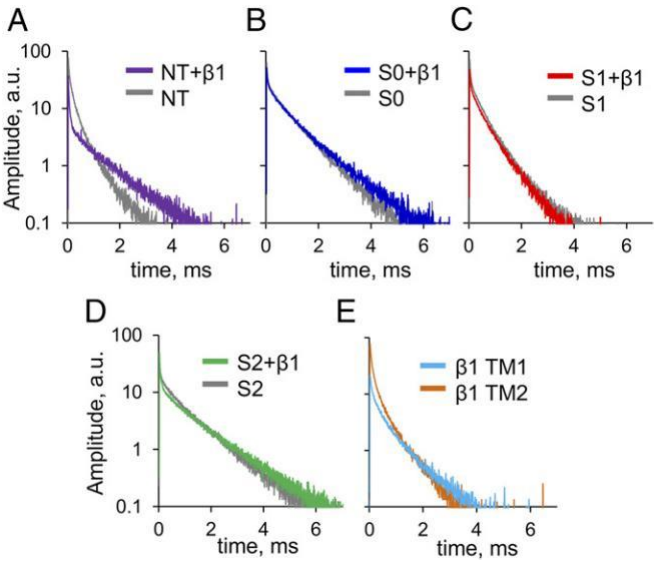

Fig. 3. LRET-based measurements reveal a rearrangement of the BK α-subunit when coexpressed with the β1-subunit. Representative SE decays recorded from oocytes independently expressing the α-LBT constructs coexpressed with the β1-subunit: NT (A), S0 (B), S1 (C), and S2 (D). For comparison, each panel shows in gray a representative SE trace of the cor-responding construct expressed without the β1-subunit. Visual inspection shows that the most dramatic changes of LRET measurements occur in the NT construct. (E) SE from oocytes independently coexpressing the WT BK α-subunit with TM1 and TM2. Different kinetics indicate that the donors of these constructs are located in different parts of the channel structure.

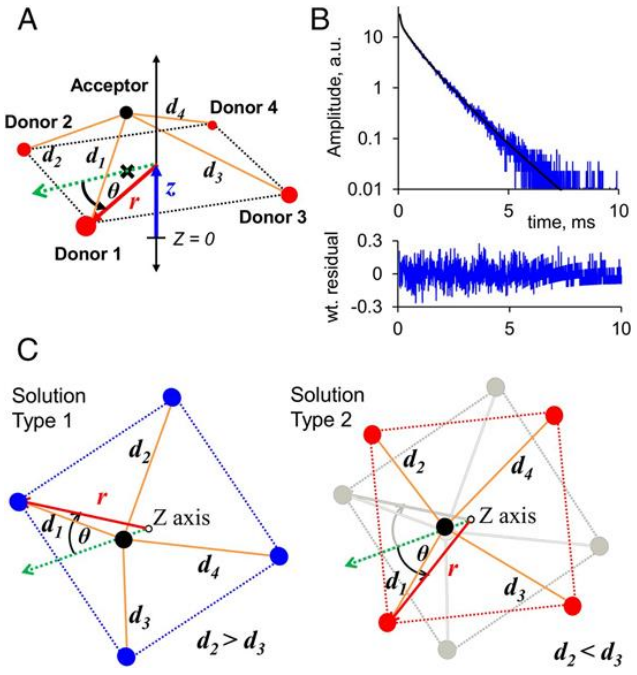

Fig. 4. Geometric model used to fit experimental SE traces. (A) Three cylindrical coordinates, r (red arrow), θ (black arc), and z (blue arrow), determine the position of the four donors (red circles) with respect to the acceptor position (black circle). The SNPS fitting program calculates four effective distances (d_1 through d_4, orange lines) that determine the shape of the theoretical SE decay according to Eqs. S1–S3 (SI Text, S1. LRET Calculations). The black cross is the projection of the acceptor cloud center of mass onto the x–y plane containing the four donors. (B) Geometric fit to a single S0 construct SE decay (Top) and weighted (wt.) residuals (Bottom). Goodness of fit is evaluated with the reduced chi square (χ^2_{RG}) value. a.u., ar-bitrary units. (C) Two equivalent geometric solutions are possible from a single fit, because the rotation angle may be ±θ with respect to the acceptor position.

four donors are in the corners of a square pyramid base and the acceptor is above them at the apex (Fig. 4). The SNPS method finds the geometric configuration yielding theoretical SE decays that best fit an ensemble of experimental SE decays (13) (details are pro-vided in SI Text, S1. LRET Calculations). The position of the ac-ceptor was modeled from the available structure of CTX bound to the Kv1.2/2.1 paddle chimera (22), and thus acts as an absolute reference point for the position of the four donors with respect to the channel pore. Donor cylindrical coordinates determined by the SNPS are detailed in Table 1. This model yields two geometrically equivalent solutions corresponding to cases where intermediate distances are related by $d_2 > d_3$ (type 1) or $d_2 < d_3$ (type 2) (Fig. 4C).

Despite this apparent ambiguity, it is possible to discard one of the two by comparing the resulting donor positions with the Kv1.2/2.1 crystal structure reference, assuming that the VSD of the BK channel keeps the basic VSD geometry. Furthermore there is no ambiguity for the case where the donor is near the symmetry line.

To summarize the selected LRET-SNPS results in the absence of the β1-subunit, Fig. 5A shows the relative position of donors for the four α-LBT constructs in the x–y plane, including 95% confi-dence isosurfaces. The donor of the S2 construct is located at the periphery of the channel at 38.9 Å from the pore axis, being the farthest of the four constructs from the symmetry axis of the channel. The S1 donor is the closest to the pore axis, with a radial distance of 29.2 Å. The S0 donor is located at 33.8 Å from the pore axis, between the S1 and S2 donors. Surprisingly, the NT donor appears to be far from the S0 donor, displaced by ~23 Å in the x–y plane projection. When compared against the Kv1.2/2.1-CTX structure, the NT and S2 donors present no rotational ambiguity, whereas for the S1 construct, only solution type 2 fits over the VSD structure near the top of the S1 segment (Fig. S3A). Only the S0 construct displayed rotational ambiguity such that both solutions are equally probable, yet they are very close to the symmetry line (Fig. S3). Fig. 5B shows a lateral view of donor positions for the four constructs tested (x–y plane projection), where differences in the relative height of the donors can be observed.

The External Architecture of the BK α/β1-Complex. As expected by the changes observed in the SE kinetics, coexpression with the β1-subunit causes a change in the pattern of donor positions (Fig. 5 C and D). Donor solution types were selected to be most parsimonious with respect to the results obtained in the absence of the β1-subunit. For instance the S2 and NT constructs showed no rotational am-biguity, whereas S1 was kept as solution type 2 for the sake of parsimony. The solution type for the S0 donor coexpressed with β1 was selected as solution type 1 because (i) a counterclockwise rotation would place the S0 segment further into the VSD, which is not likely, and (ii) this solution type better agrees with reported interactions between the S0 segment and the TM1 or TM2 segment of the β1-subunit (24, 25). For the TM1 and TM2 constructs, the best choice was solution type 1; otherwise, these segments would be positioned inside the voltage sensor, a solution that has no physical meaning (Fig. 5C and Fig. S3B). The spatial map of Fig. 5 C and D shows that both the TM1 and TM2 donors are positioned between adjacent subunit VSDs and in the vicinity of the S0 donor, radially closer to the pore axis by 0.4 Å and 4 Å, respectively.

We noted that by maintaining the acceptor static, the donor position of all constructs except S1 clashed with an upper height boundary equal to the height of the acceptor. Because this picture seems unlikely, we shifted the acceptor position 1 Å radially out-ward from the pore axis for the complete dataset in the presence of the β1-subunit. The result was an overall decrease in individual fit

Table 1. Donor coordinates of BK-LBT constructs determined by nanopositioning (SNPS)

Construct	Solution	r (Å)	θ (º)*	z (Å)	χ^2_{RG}	n
S0	2	33.8 (−1.4, +1.2)	1.7 (−17.8,† +14.4)	24.4 (−3.1, +3.6)	1.028	18
S1	2	29.2 (−1.2, +1.1)	12.9 (−12.9, +11.6)	23.3 (−2.4, +2.7)	1.022	17
S2	2	38.9 (−0.8, +0.1)	0.0 (−14.2,† +14.2)	37.3 (−7.4, +7.4)	1.025	11
NT	2	33.1 (−1.0, +0.3)	45.0 (−8.2, +8.2)	37.3 (−8.4, +8.3)	1.039	8
S0+β1	2	35.1 (−1.2, +1.2)	10.8 (−10.8, +10.3)	24.3 (−2.6, +3.3)	1.019	7
S1+β1	2	24.2 (−1.4, +1.1)	23.3 (−11.9, +16.9)	15.4 (−1.5, +1.3)	1.026	20
S2+β1	2	43.4 (−1.2, +0.1)	0.0 (−10.1,† +10.1)	37.3 (−9.6, +9.5)	1.027	5
NT+β1	2	41.9 (−1.2, +0.2)	0.0 (−10.9,† +10.9)	37.3 (−9.6, +9.5)	1.045	13
αBK + β1TM1	1	35.5 (−0.9, +0.4)	−22.7 (−13.3, +12.2)	37.4 (−7.6, +7.5)	1.026	6
αBK + β1TM2	1	31.1 (−1.5, +1.5)	−27.8 (−10.1, +5.2)	26.4 (−4.2, +8.7)	1.039	3

*Rotation angle is relative to acceptor position: (x,y,z) = (−2.20,−4.21,37.36) Å, in absence of β1.
†Confidence region crossed over into opposite solution space.

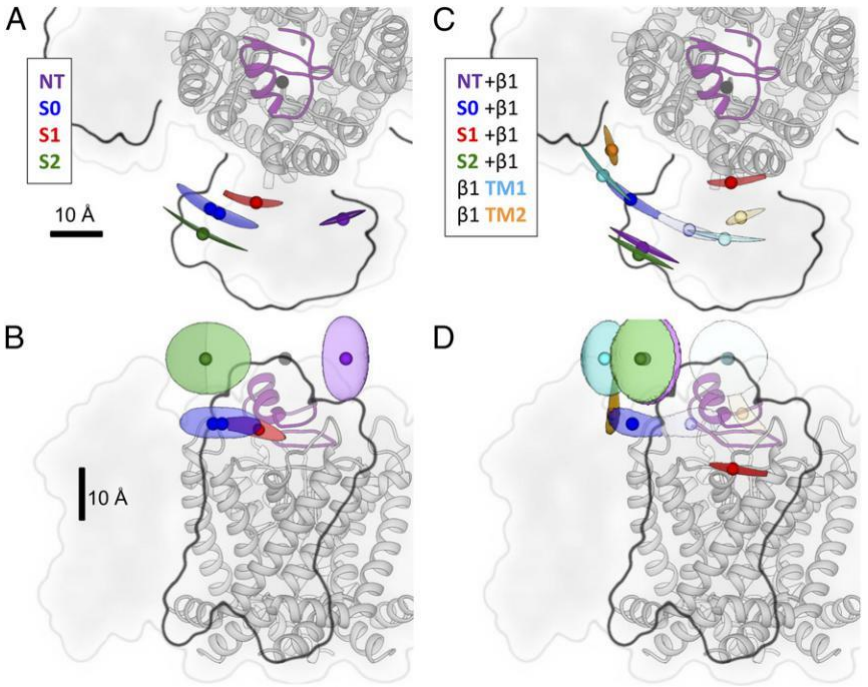

Fig. 5. Spatial map of the extracellular face of the BK VSD obtained from the geometric fit to SE traces. The position of each donor is represented by colored filled circles. The 95% confidence isosurfaces are shown as transparent volumes. For the sake of clarity, the donors from only one subunit are shown. The reference point is the acceptor (black circle) near the fourfold symmetry axis. The crystal structure of the pore section from the Kv1.2/2.1 paddle chimera (transparent gray) and the modeled IbTX-bodipy (purple) are presented in the background as references. The tentative area where the bulk of the BK VSD may be located is encircled by a black line. The space-filled boundary of the Kv1.2/2.1 paddle chimera is shown as a fainter gray line. (A and B) Top and side views, respectively, of the spatial map for BK constructs in the absence of the β1-subunit. (C and D) Top and side views, respectively, of the spatial map for BK constructs in the presence of the β1-subunit. Donors from the β1-LBT constructs TM1 and TM2 are shown as cyan and orange circles, respectively. For completeness, both solution types are shown for S0 + β1, TM1, and TM2 constructs. However, the less likely solutions are rendered transparent to reinforce the fact that they appear nonparsimonious.

error and the spreading of donor positions in the z axis (Fig. S4). This operation results in a more physically meaningful picture; therefore, the reported results in Fig. 5 C and D consider the shifted position of the acceptor, although this shift implies a slight change in the acceptor position due to the presence of the β1-subunit.

The most dramatic structural rearrangement induced by the presence of the β1-subunit is the NT construct with a 29.8-Å displacement in the x–y plane. This rearrangement places the NT donor very near the new position of the S2 construct. At the same time, the S2 construct undergoes a displacement of 4.5 Å in the x–y plane away from the pore axis. The S1 construct shows a displacement toward the pore axis of 5 Å and a counterclockwise rotation of 10°. Finally, S0 moves 5.6 Å in the x–y plane with a clockwise rotation away from the S1 and S2 donors (S0 solution type 1 as a reference). Changes in the z-coordinate of each donor can also be observed. In particular, a downward displacement of the S1 donor by 7.9 Å is the most remarkable vertical shift. In contrast, NT, S0, and S2 have little change in the z-coordinate (<0.2 Å) when coexpressed with the β1-subunit. Fig. 6 summarizes the position changes of the donors in the α-subunit as a result of coexpressing the β1-subunit, as well as the position of the TM1 and TM2 donors of the β1-subunit.

Discussion

Different from all other members of the Kv channels superfamily, in BK channels, not only the S4 segment but also the S2 and S3 segments of the VSD carry the electric charges that sense the membrane electric field (26–28). The translocation of these charged residues in the membrane electric field induces conformational changes in the VSD that can be tracked with site-directed voltage-clamp fluorometry (29–31). BK channels also have the additional S0 transmembrane segment preceding the six canonical segments (10, 11). Tryptophan scanning mutagenesis in S0 and fluorescence quenching by tryptophan W203 in the S3–S4 linker suggest that the NT of the S0 segment is in close contact with the VSD (S1–S4). This interaction would modulate the equilibrium between the resting and active states of the voltage sensor (32, 33).

Little is known about the detailed structure of the transmembrane portion of the BK channel, although some initial glimpses of the channel's structure have been given using cryoelectron microscopy at a resolution of 17 Å (34). The BK structure resolved by this technique shows a large protrusion at the periphery of the VSD at ~40 Å radial from the pore axis, which should correspond to the additional S0 helix and ~40 extracellular N-terminal residues of the BK α-subunit. This observation is in good agreement with our measurement using LRET that places the S0 donor 33.8 Å radial from the pore axis.

BK Transmembrane Segments Pattern. Information about the relative position of transmembrane segments was reported by using disulfide cross-linking experiments. There, S0 appeared to lie in close proximity to the S3–S4 loop, near the S1 and S2 segments and away from the S5 and S6 segments, based on the extent of disulfide bond formation between introduced cysteine residues (35). The best way to interpret these data was by positioning S0 surrounded by all the other transmembrane segments of the voltage sensor (S1– S4), preventing S0 from making contact with segments S5 and S6. More recently, using voltage-clamp fluorometry, it was found that a fluorescent label on the extracellular side of the S0 segment can be quenched by tryptophan W203 of the S3–S4 loop in a state-dependent manner, supporting the proximity of the S0 segment with the S3–S4 loop in the resting state (30). Using the same approach, after strategically locating the fluorescent probe and by introducing or substituting the quencher tryptophan, it was concluded that the

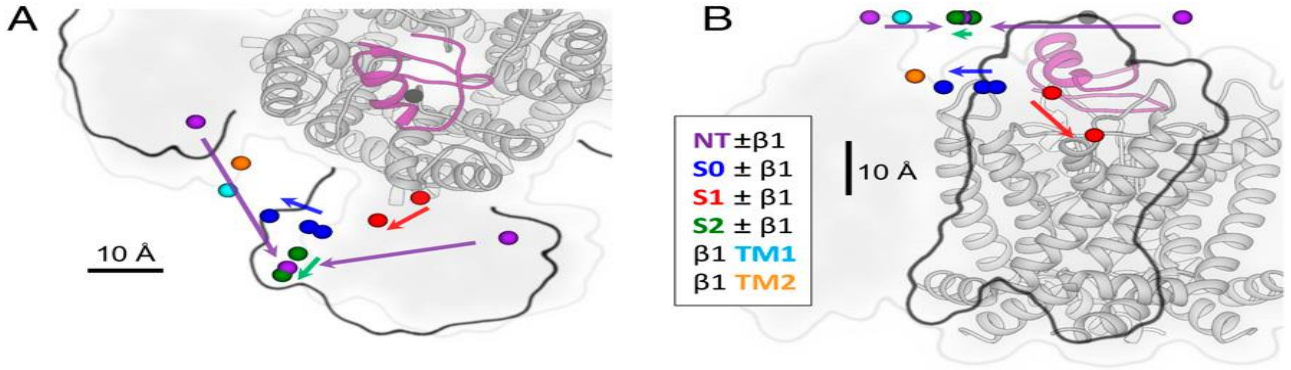

Fig. 6. Change in the donor position due to the presence of the β1-subunit. (A and B) Top and side views, respectively, of the changes in the donor positions as a consequence of coexpression with the β1-subunit. The 95% confidence isosurfaces are not displayed for clarity. Colored arrows indicate the direction of the change in position.

S1 segment would be closer to W203 (which would be in close proximity to S0) than the S2 segment in the resting state (31). Our results place the position of the S0 donor nearly in-line between S1 and S2: a distance of 7.7 Å from S1 and 5.2 Å from S2 in the x–y plane (Fig. 5A).

The Transmembrane Segments Pattern of the BK α/β1-Complex. The β1-subunit consists of two putative transmembrane segments joined together by a large extracellular loop (36). The BK β1-subunit in-creases the apparent Ca^{2+} sensitivity of the channel, slows down the macroscopic activation and deactivation kinetics, and decreases the voltage sensitivity (37–44). By stabilizing the voltage sensor in its active configuration, the β1-subunit has an important effect on the BK channel's apparent Ca^{2+} sensitivity (43, 45). Therefore, it is reasonable to think that there is a close spatial relationship be-tween the β1-subunit's transmembrane segments and the VSD of the α-subunit. Our LRET experiments show that the α-subunit undergoes a change in the spatial pattern of its transmembrane segments when coexpressed with the β1-subunit (Fig. 5).

Using the disulfide cross-linking technique, Marx and co-workers (24, 25) also described the spatial distribution of BK transmembrane segments in the presence of the β1-subunit. Surprisingly, to best account for the results reported by Liu et al. (25), they no longer positioned the S0 segment surrounded by the other four trans-membrane segments but in the periphery of the VSD facing the S3 and S4 segments. Their model does not allow direct contact of S0 with the S1 and S2 segments even though their results showed be-tween 40% and 80% disulfide cross-linking between S0 and the S1 and S2 segments (25). In contrast, our results place the S0 segment in close proximity (<7 Å) to the S1 and S2 segments. In their work, the extent of cross-linking is only interpreted as relative differences in distances between cysteine residues, and the estimation is done a long time after cross-linking occurs. In contrast, our LRET mea-surements are performed in real time, with functional channels expressed in the membrane of a living cell, and the retrieved posi-tions of donors anchored to the different transmembrane segments rely only on the modeled acceptor position and assumed fourfold channel symmetry (13).

Disulfide cross-linking between the β1-subunit and α-subunit suggested that both TM1 and TM2 segments are in close proximity to S0, S1, and S2; however disulfide bond formation is essentially prevented for the S3 to S6 segments (24, 25). This finding is con-sistent with our proposed location for the TM1 and TM2 segments, which appear adjacent to the S0-NT position (Fig. 5 C and D), and show that TM1 is 2.4 Å closer to S0 than TM2 in the x–y projection. These observations could give structural support to functional coupling between the S0/NT of the BK α-subunit and the β1-sub-unit (46). Due to the short distance to S0, TM1 is likely making contact with the α-subunit at this point, and these contacts may be responsible for the observed changes in the biophysical properties of the BK channel when coexpressed with the β1-subunit. Also, consistent with results reported by Liu et al. (25), our LRET ex-periments locate the TM1 and TM2 segments at the interface of adjacent voltage sensing domains (Fig. 5C), with both segments close to each other, allowing disulfide bond formation between these two segments.

A Model Structure of the External Aspect of the BK Channel. To ac-count for our LRET findings in the structural context, we performed an LBT position-restrained MD protocol to refine a BK homology model according to our calculated donor positions (details are provided in Experimental Procedures). The BK structural model obtained using this approach is shown in Fig. 7A. The positions of segments S0, S1, and S2 are in agreement with these segments' interactions reported previously (35). However, in our molecular model, the S0 segment is closer to the S1 and S2 segments than to the S3 and S4 segments.

To have the complete picture, we also performed a position-restrained model of the BK channel using the donor coordinates obtained in the presence of the β1-subunit (Fig. 7B). The structural changes in the BK model due to the presence of the β1-subunit are detailed in Fig. 7 C and D, including the transmembrane segments TM1 and TM2 docked in such a way that they best match LRET results. As a measure of β1-induced conformational change, we calculated the rmsd between the two models as 2.7 Å for the whole channel, 3.3 Å considering only the VSD (S0–S4), and 0.8 Å con-sidering only the pore section (S5–S6). Our LRET-restrained model locates both the TM1 and TM2 segments of the β1-subunit near S0 and S1 in the space between two adjacent voltage sensors. This vicinity allows interaction between both transmembrane segments and also prevents interaction with S3–S4 segments as proposed by Liu et al. (24, 25).

The presence of the β1-subunit not only modifies the operation of the VSD but also dramatically slows the activation and deactivation kinetics (41, 43, 45, 47). The reported crucial role of the cytoplasmic domains of β-subunits (48, 49) requires close proximity of both cy-toplasmic domains of the β1-subunit and the α-subunit VSDs. The molecular model proposed here for the BK α/β1-complex inferred from LRET experiments allows such interactions, given that the transmembrane segments of the α- and β1-subunits are close to each other.

Experimental Procedures

Donors and Acceptors. The LBT, sequence YIDTNNDGWYEGDELLA (18), was inserted in chosen positions of the BK channel. LBT-BK channels were constructed using standard molecular biology techniques and a site-directed mutagenesis kit (QuikChange; Stratagene). Correct insertion of LBTs was confirmed by sequenc-ing. As the LRET acceptor, we used the fluorophore bodipy attached to the peptidic scorpion toxin IbTX, a high-affinity pore blocker of BK channels. Labeled

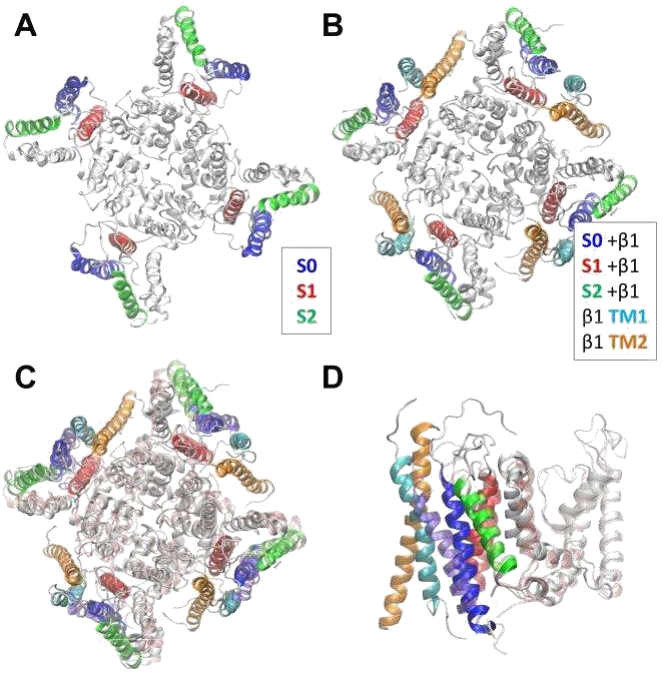

Fig. 7. LRET-restrained molecular model of the BK channel. LBT insertions were sequentially included (one at a time) in LRET-restrained MD simulations used to construct the BK model. (A) Top view of the BK model in the absence of the β1-subunit. (B) Top view of the BK model in the presence of the β1-subunit. (C and D) Top and side views, respectively, of the BK model in the presence of the β1-subunit (solid white) compared with the model in its absence (trans-parent pink). The side view (D) includes only one subunit for clarity. The TM1 and TM2 segments were docked to match best the donor position obtained from β1-LBT constructs. LBT-labeled helices are colored consistent with LBT construct colors used throughout the paper.

[D19C]IbTX was custom-synthesized in solid phase, and bodipy fluorophore was also custom-synthesized in-house (SI Text, S2. IbTX-Bodipy Synthesis and Fig. S5). We determined the Förster distance to be $R_0 \approx 39.7$ Å for the LBT-Tb^{3+}/[D19C] IbTX-bodipy pair (SI Text, S1. LRET Calculations).

Heterologous Protein Expression Electrophysiology. For BK expression in oocytes, the WT and mutant channels' cDNA was transcribed using an in vitro T7 poly-merase transcription kit (Ambion). The transcribed cRNA (50 ng) was injected into Xenopus oocytes. Oocytes were incubated in SOS (100 mM NaCl, 2 mM KCl, 1.8 mM $CaCl_2$, 1 mM $MgCl_2$, 5 mM Hepes, pH 7.6) or ND96 (96 mM NaCl, 2 mM KCl, 1 mM $CaCl_2$, 1 mM $MgCl_2$, 5 mM Hepes, pH 7.6) solution at 18 °C for 3–5 d before recording. For electrophysiological characterization of BK-LBT constructs, patch-clamp experiments were performed with an Axopatch 200B amplifier in an inside-out configuration. The bath and pipette solution both contained 110 mM K-MES, 10 mM Hepes, and 5 mM EGTA (pH 7.4). In LRET experiments, a CA-1B amplifier (Dagan Corp.) in a two-electrode voltage-clamp configuration was used to keep the transmembrane voltage fixed at −80 mV. The internal microelectrodes' resistance was 0.4–0.8 MΩ, and the pipette solution was 3 M KCl. For donor emission experiments, the bath solution composition was 110 mM N-methyl-D-glucamine-methanosulfonic acid, 10 mM Hepes, 2 mM $CaCl_2$, and 10 μM $TbCl_3$ (pH 7.4). For acceptor-SE experiments, the bath solution additionally contained 500 nM IbTX-bodipy. The acceptor-containing solution was made by adding 3 μL of 20 μM IbTX-bodipy solution to 117 μL of DO solution. Oocytes were incubated for 5–15 min in the IbTX-bodipy–containing solution before SE recording.

Optical Setup. The optical setup used for simultaneous LRET and electrophysiology experiments was custom-designed and has been described before (13, 19). Briefly, to excite the donor, we used a 5-ns pulse at the 266-nm line of a qua-drupled neodymium-yttrium aluminium garnet (Nd:YAG) laser (Spectra Physics). The laser excitation beam passes through excitation optics composed of a fused silica Pellin–Broca prism (Thorlabs) and UG11 cleanup filter, followed by a custom 266-nm laser dichroic with no antireflection (AR)-coating (Z266rdc; Chroma Technology). A 40× (1.25 N.A.) glycerol immersion quartz objective with no AR-coating (Partec GmbH) was used to collect the light from the sample. Emission filters were a long-pass E515LPv2 or a band-pass D520/20m (Chroma Technol-ogy) for DO emission or SE recordings, respectively. The optical signal was detected with a gated photomultiplier tube (Hamamatsu) coupled to a custom-made current/voltage converter. Analog fluorescence signal was filtered with an eight-pole Bessel filter at either 50 kHz or 100 kHz cutoff frequency, and acquired with a sample period of 2 μs using a 14-bit analog-to-digital converter. DO and SE traces were obtained by averaging 16–25 pulses.

SE Analysis. Geometric models for all constructs were obtained by analyzing their respective SE decay measurements. The analysis was performed using the SNPS software developed by our group (13) using MATLAB (MathWorks). Briefly, the program generates a theoretical SE signal from a geometric model that takes into account the position of the four Tb^{3+} donors and the single acceptor in a pyramid-like model (Fig. 4A). The program routine finds the best geometry that simultaneously fits multiple experimental SE traces of a given LBT construct and conformational state. Solution types of the geometric model were selected according to the reference Kv1.2/2.1-CTX structure. Selection was made to have maximal overlap between the donor positions and the VSD of the paddle chimera. Details of this procedure can be found in SI Text, S1. LRET Calculations.

Acceptor Position Sampling by Dihedral Angle Scan. The conformational space of bodipy within the [D19C]IbTX–bodipy–BK complex model (SI Text, S3. Molecular Modeling and MD Simulations) was sampled by scanning the flu-orophore–toxin complex dihedral angles Ψ_1, Ψ_2, Ψ_3, and Ψ_4 defined in Fig. S6A using 30° increments per dihedral (e.g., $\Psi_1 = -150°, -120°, \ldots, 180°$). The scanned sample consists of 20,736 structures, which were evaluated in terms of their van der Waals (vdW) energy to discard clashed conformations (E_{vdW} > 1,000 kcal/mol or atomic distances < 1.4 Å). Each of the resulting 3,290 con-formations was used to represent the accessible or diffusive volume of bodipy's transition dipole moment (estimated as the geometric center of the chromo-phore's central ring), such that each valid conformation is represented by a point, which, together, define the acceptor (cloud) position within the reference frame of the IbTX–BK complex (Fig. S6C).

LRET-Restrained Molecular Modeling of BK. Donor coordinates obtained from geometric fits to SE data were used as a constraint to refine an initial BK α-subunit model in the absence of the β1-subunit (SI Text, S3. Molecular Modeling and MD Simulations). The LBT peptide sequence was inserted into target sites accordingly to reproduce the LBT-BK constructs in silico using the same MD simulation size and parameters described for the [D19C]IbTX–bodipy–BK complex.

An LBT-Tb^{3+}-restrained MD protocol was performed to refine the BK model according to donor coordinates. The Tb^{3+} Cartesian coordinates were restrained to its donor experimental position by means of a harmonic potential of 1 or 2 kcal·mol^{-1}·Å^2 using the colvar module of NAMD 2.9. The use of positional restraints allows smooth adaptation of the LBT-Tb^{3+} and the attached BK segment to the SNPS results. To maintain the LBT structure, a restraint of 2 kcal·mol^{-1}·Å^2 was also applied between the calcium (representing the terbium donor atom) and LBT's charged side-chains.

Each LBT-BK system was simulated independently. The first system assembled included the LBT at the S1 insertion site. The positions of all four donor atoms were simultaneously restrained by coordinates obtained from the geometric fit. After 28 ns of simulation, the LBT structures were removed from S1 and inserted into the S2 site, extending the simulation by 28 ns with the donor positions restrained accordingly. Following the same strategy, the LBTs were inserted at the S0 site and simulated for 28 ns. The NT-LBT system was not simulated due to the intrinsic freedom of the NT. Finally, the LBTs were removed and the system was further relaxed for 40 ns.

Once each LBT segment was located at its experimental position by the above procedure, the subunit with the lowest energy conformation was considered to build a symmetrical tetramer of the BK α-subunit. The new symmetrical tetramer was used to build a membrane-embedded channel molecular system with the same dimensions and characteristics described above, and submitted to an MD simulation with restrained secondary structure. Symmetry was retained by means of harmonic restraints. The final production simulation lasted 20 ns.

The aforementioned BK channel was used to construct a 3D structural model of the BK α/β1-complex. The transmembrane segments of the β1-subunit were modeled using a generic α-helix due to lack of a crystal structure. The β1-subunit sequence obtained from the UniProt database (ID code Q16558) was analyzed using three secondary structure prediction algorithms [PSIPRED (50), MEMSAT (51) and TMHMM (52)] to define the transmembrane segments' residues. The segments were modeled using the Prime module from the Schrödinger Suite, followed by a 5-ns MD protocol with the segments embedded in a phosphatidyloleoyl phosphatidylcholine (POPC) hydrated

.

Both α- and β1-subunits were embedded in a POPC hydrated bilayer with 150 mM KCl. To represent the β1-subunit TM position calculated by LRET experiments, the α-carbon of the first residue of each segment was restricted to the x–y coordinates of its corresponding experimentally determined position (Ser45 for TM1 and Pro164 for TM2). This conformation was selected over other β1-subunits to minimize possible steric clashes among the extracellular loops. The final system containing BK α/β1-complex (final size of 210 × 210 × 111 $Å^3$, total of 371,560 atoms) was submitted to a 20-ns MD protocol using secondary and symmetry restraints as described above.

ACKNOWLEDGMENTS. We thank Boris Horvath Dreyer (UMass Amherst) for obtaining the NMR structure and assistance with peptide purification and characterization. This research was supported by Fondo Nacional de Desarrollo Científico y Tecnológico Grants 1110430 and 1150273 (to R.L.), 1131003 (to F.D.G.-N.), and 11130576 (to D.A.); Anillo Grant ACT-1107, Comisión Nacional de Investigación Científica y Tecno-lógica (CONICYT) - Programa de Investigación Asociativa (PIA) (to F.D.G.-N.); NIH Grant GM030376 (to F.B.); and NIH U54GM087519 (to F.B.); a CONACYT post-doctoral fellowship, Mexican Government (to J.E.S.-R.); CONICYT Graduate Fel-lowship 21090197 and Grant AT-24121240 (to J.P.C.); and CONICYT Grant 21130631, Chilean Government (to R.S.). The Centro Interdisciplinario de Neurociencia de Valparaiso is a Millennium Institute supported by the Mil-lennium Scientific Initiative of the Chilean Ministry of Economy, Develop-ment, and Tourism (P029-022-F).

1. Contreras GF, et al. (2013) A BK (Slo1) channel journey from molecule to physiology. Channels (Austin) 7(6):442–458.
2. Cui J, Yang H, Lee US (2009) Molecular mechanisms of BK channel activation. Cell Mol Life Sci 66(5):852–875.
3. Latorre R, Brauchi S (2006) Large conductance Ca2+-activated K+ (BK) channel: Activation by Ca2+ and voltage. Biol Res 39(3):385–401.
4. Orio P, Rojas P, Ferreira G, Latorre R (2002) New disguises for an old channel: MaxiK channel beta-subunits. News Physiol Sci 17:156–161.
5. Sun X, Zaydman MA, Cui J (2012) Regulation of Voltage-Activated K(+) Channel Gating by Transmembrane β Subunits. Front Pharmacol 3:63.
6. Toro L, Wallner M, Meera P, Tanaka Y (1998) Maxi-K(Ca), a Unique Member of the Voltage-Gated K Channel Superfamily. News Physiol Sci 13:112–117.
7. Torres YP, Morera FJ, Carvacho I, Latorre R (2007) A marriage of convenience: Beta-subunits and voltage-dependent K+ channels. J Biol Chem 282(34):24485–24489.
8. Yan J, Aldrich RW (2010) LRRC26 auxiliary protein allows BK channel activation at resting voltage without calcium. Nature 466(7305):513–516.
9. Yan J, Aldrich RW (2012) BK potassium channel modulation by leucine-rich repeat-containing proteins. Proc Natl Acad Sci USA 109(20):7917–7922.
10. Meera P, Wallner M, Song M, Toro L (1997) Large conductance voltage- and calcium-dependent K+ channel, a distinct member of voltage-dependent ion channels with seven N-terminal transmembrane segments (S0-S6), an extracellular N terminus, and an intracellular (S9-S10) C terminus. Proc Natl Acad Sci USA 94(25):14066–14071.
11. Wallner M, Meera P, Toro L (1996) Determinant for beta-subunit regulation in high-conductance voltage-activated and Ca(2+)-sensitive K+ channels: An additional transmembrane region at the N terminus. Proc Natl Acad Sci USA 93(25):14922–14927.
12. Cha A, Snyder GE, Selvin PR, Bezanilla F (1999) Atomic scale movement of the voltage-sensing region in a potassium channel measured via spectroscopy. Nature 402(6763): 809–813.
13. Hyde HC, et al. (2012) Nano-positioning system for structural analysis of functional homomeric proteins in multiple conformations. Structure 20(10):1629–1640.
14. Posson DJ, Ge P, Miller C, Bezanilla F, Selvin PR (2005) Small vertical movement of a K+ channel voltage sensor measured with luminescence energy transfer. Nature 436(7052):848–851.
15. Posson DJ, Selvin PR (2008) Extent of voltage sensor movement during gating of shaker K+ channels. Neuron 59(1):98–109.
16. Richardson J, et al. (2006) Distance measurements reveal a common topology of prokaryotic voltage-gated ion channels in the lipid bilayer. Proc Natl Acad Sci USA 103(43):15865–15870.
17. Selvin PR (2002) Principles and biophysical applications of lanthanide-based probes. Annu Rev Biophys Biomol Struct 31:275–302.
18. Nitz M, et al. (2004) Structural origin of the high affinity of a chemically evolved lanthanide-binding peptide. Angew Chem Int Ed Eng, 4328, pp 3682–3685.
19. Sandtner W, Bezanilla F, Correa AM (2007) In vivo measurement of intramolecular distances using genetically encoded reporters. Biophys J 93(9):L45–L47.
20. Candia S, Garcia ML, Latorre R (1992) Mode of action of iberiotoxin, a potent blocker of the large conductance Ca(2+)-activated K+ channel. Biophys J 63(2):583–590.
21. Galvez A, et al. (1990) Purification and characterization of a unique, potent, peptidyl probe for the high conductance calcium-activated potassium channel from venom of the scorpion Buthus tamulus. J Biol Chem 265(19):11083–11090.
22. Banerjee A, Lee A, Campbell E, Mackinnon R (2013) Structure of a pore-blocking toxin in complex with a eukaryotic voltage-dependent K(+) channel. eLife 2:e00594.
23. Heyduk T, Heyduk E (2001) Luminescence energy transfer with lanthanide chelates: Interpretation of sensitized acceptor decay amplitudes. Anal Biochem 289(1):60–67.
24. Liu G, et al. (2008) Locations of the beta1 transmembrane helices in the BK potassium channel. Proc Natl Acad Sci USA 105(31):10727–10732.
25. Liu G, et al. (2010) Location of modulatory beta subunits in BK potassium channels. J Gen Physiol 135(5):449–459.
26. Díaz L, et al. (1998) Role of the S4 segment in a voltage-dependent calcium-sensitive potassium (hSlo) channel. J Biol Chem 273(49):32430–32436.
27. Cui J, Aldrich RW (2000) Allosteric linkage between voltage and Ca(2+)-dependent activation of BK-type mslo1 K(+) channels. Biochemistry 39(50):15612–15619.
28. Ma Z, Lou XJ, Horrigan FT (2006) Role of charged residues in the S1-S4 voltage sensor of BK channels. J Gen Physiol 127(3):309–328.
29. Pantazis A, Gudzenko V, Savalli N, Sigg D, Olcese R (2010) Operation of the voltage sensor of a human voltage- and Ca2+-activated K+ channel. Proc Natl Acad Sci USA 107(9):4459–4464.
30. Pantazis A, Kohanteb AP, Olcese R (2010) Relative motion of transmembrane segments S0 and S4 during voltage sensor activation in the human BK(Ca) channel. J Gen Physiol 136(6):645–657.
31. Pantazis A, Olcese R (2012) Relative transmembrane segment rearrangements during BK channel activation resolved by structurally assigned fluorophore-quencher pair-ing. J Gen Physiol 140(2):207–218.
32. Koval OM, Fan Y, Rothberg BS (2007) A role for the S0 transmembrane segment in voltage-dependent gating of BK channels. J Gen Physiol 129(3):209–220.
33. Semenova NP, Abarca-Heidemann K, Loranc E, Rothberg BS (2009) Bimane fluorescence scanning suggests secondary structure near the S3-S4 linker of BK channels. J Biol Chem 284(16):10684–10693.
34. Wang L, Sigworth FJ (2009) Structure of the BK potassium channel in a lipid membrane from electron cryomicroscopy. Nature 461(7261):292–295.
35. Liu G, et al. (2008) Position and role of the BK channel alpha subunit S0 helix inferred from disulfide crosslinking. J Gen Physiol 131(6):537–548.
36. Knaus HG, et al. (1994) Primary sequence and immunological characterization of beta-subunit of high conductance Ca(2+)-activated K+ channel from smooth muscle. J Biol Chem 269(25):17274–17278.
37. Wallner M, et al. (1995) Characterization of and modulation by a beta-subunit of a human maxi KCa channel cloned from myometrium. Receptors Channels 3(3):185–199.
38. Orio P, Latorre R (2005) Differential effects of beta 1 and beta 2 subunits on BK channel activity. J Gen Physiol 125(4):395–411.
39. Nimigean CM, Magleby KL (2000) Functional coupling of the beta(1) subunit to the large conductance Ca(2+)-activated K(+) channel in the absence of Ca(2+). Increased Ca(2+) sensitivity from a Ca(2+)-independent mechanism. J Gen Physiol 115(6):719–736.
40. Meera P, Wallner M, Jiang Z, Toro L (1996) A calcium switch for the functional cou-pling between alpha (hslo) and beta subunits (Kv,cabeta) of maxi K channels. FEBS Lett 385(1-2):127–128.
41. Dworetzky SI, et al. (1996) Phenotypic alteration of a human BK (hSlo) channel by hSlobeta subunit coexpression: Changes in blocker sensitivity, activation/relaxation and inactivation kinetics, and protein kinase A modulation. J Neurosci 16(15):4543–4550.
42. Cox DH, Aldrich RW (2000) Role of the beta1 subunit in large-conductance Ca(2+)-activated K (+) channel gating energetics. Mechanisms of enhanced Ca(2+) sensitivity. J Gen Physiol 116(3):411–432.
43. Bao L, Cox DH (2005) Gating and ionic currents reveal how the BKCa channel's Ca2+ sensitivity is enhanced by its beta1 subunit. J Gen Physiol 126(4):393–412.
44. McManus OB, et al. (1995) Functional role of the beta subunit of high conductance calcium-activated potassium channels. Neuron 14(3):645–650.
45. Contreras GF, Neely A, Alvarez O, Gonzalez C, Latorre R (2012) Modulation of BK channel voltage gating by different auxiliary β subunits. Proc Natl Acad Sci USA 109(46): 18991–18996.
46. Morrow JP, et al. (2006) Defining the BK channel domains required for beta1-subunit modulation. Proc Natl Acad Sci USA 103(13):5096–5101.
47. Brenner R, Jegla TJ, Wickenden A, Liu Y, Aldrich RW (2000) Cloning and functional characterization of novel large conductance calcium-activated potassium channel beta subunits, hKCNMB3 and hKCNMB4. J Biol Chem 275(9):6453–6461.
48. Orio P, et al. (2006) Structural determinants for functional coupling between the beta and alpha subunits in the Ca2+-activated K+ (BK) channel. J Gen Physiol 127(2): 191–204.
49. Castillo K, et al. (2015) Molecular mechanism underlying β1 regulation in voltage- and calcium-activated potassium (BK) channels. Proc Natl Acad Sci USA 112(15):4809–4814.
50. McGuffin LJ, Bryson K, Jones DT (2000) The PSIPRED protein structure prediction server. Bioinformatics 16(4):404–405.
51. Jones DT (2007) Improving the accuracy of transmembrane protein topology pre-diction using evolutionary information. Bioinformatics 23(5):538–544.
52. Krogh A, Larsson B, von Heijne G, Sonnhammer EL (2001) Predicting transmembrane protein topology with a hidden Markov model: Application to complete genomes. J Mol Biol 305(3):567–580.
53. Mitchell AR, Kent SBH, Engelhard M, Merrifield RB (1978) A new synthetic route to tert-butyloxycarbonylaminoacyl-4-(oxymethyl)phenylacetamidomethyl-resin, an im-proved support for solid-phase peptide synthesis. J Org Chem 43(14):2845–2852.
54. Rosenthal J, Lippard SJ (2010) Direct detection of nitroxyl in aqueous solution using a tripodal copper(II) BODIPY complex. J Am Chem Soc 132(16):5536–5537.
55. Schnölzer M, Alewood P, Jones A, Alewood D, Kent SB (1992) In situ neutralization in Boc-chemistry solid phase peptide synthesis. Rapid, high yield assembly of difficult sequences. Int J Pept Protein Res 40(3-4):180–193.
56. Schnölzer M, Alewood P, Jones A, Alewood D, Kent SH (2007) In situ neutralization in Boc-chemistry solid phase peptide synthesis. Int J Pept Res Ther 13(1-2):31–44.
57. Hackeng TM, Griffin JH, Dawson PE (1999) Protein synthesis by native chemical ligation: Expanded scope by using straightforward methodology. Proc Natl Acad Sci USA 96(18):10068–10073.

58. Purwaha P, Silva LP, Hawke DH, Weinstein JN, Lorenzi PL (2014) An artifact in LC-MS/ MS measurement of glutamine and glutamic acid: In-source cyclization to pyroglutamic acid. Anal Chem 86(12):5633–5637.
59. Nugent T, Jones DT (2009) Transmembrane protein topology prediction using support vector machines. BMC Bioinformatics 10:159.
60. Carvacho I, et al. (2008) Intrinsic electrostatic potential in the BK channel pore: Role in determining single channel conductance and block. J Gen Physiol 131(2):147–161.
61. Posson DJ, McCoy JG, Nimigean CM (2013) The voltage-dependent gate in MthK potassium channels is located at the selectivity filter. Nat Struct Mol Biol 20(2):159–166.
62. Long SB, Tao X, Campbell EB, MacKinnon R (2007) Atomic structure of a voltage-dependent K+ channel in a lipid membrane-like environment. Nature 450(7168):376–382.
63. Lu R, et al. (2006) MaxiK channel partners: Physiological impact. J Physiol 570(Pt 1):65–72.
64. Song KC, et al. (2011) Orientation of fluorescent lipid analogue BODIPY-PC to probe lipid membrane properties: Insights from molecular dynamics simulations. J Phys Chem B 115(19):6157–6165.
65. Johnson BA, Sugg EE (1992) Determination of the three-dimensional structure of iberiotoxin in solution by 1H nuclear magnetic resonance spectroscopy. Biochemistry 31(35):8151–8159.
66. Sali A, Blundell TL (1993) Comparative protein modelling by satisfaction of spatial restraints. J Mol Biol 234(3):779–815.
67. Giangiacomo KM, et al. (2008) Novel alpha-KTx sites in the BK channel and comparative sequence analysis reveal distinguishing features of the BK and KV channel outer pore. Cell Biochem Biophys 52(1):47–58.
68. Phillips JC, et al. (2005) Scalable molecular dynamics with NAMD. J Comput Chem 26(16):1781–1802.
69. Klauda JB, et al. (2010) Update of the CHARMM all-atom additive force field for lipids: Validation on six lipid types. J Phys Chem B 114(23):7830–7843.
70. Feller SE, Zhang Y, Pastor RW, Brooks BR (1995) Constant pressure molecular dynamics simulation: The Langevin piston method. J Chem Phys 103:4613–4621.
71. Wells DB, et al. (2012) Optimization of the molecular dynamics method for simula-tions of DNA and ion transport through biological nanopores. Methods Mol Biol 870: 165–186.
72. Jorgensen W, Madura J (1983) Quantum and statistical mechanical studies of liq-uids. 25. Solvation and conformation of methanol in water. J Am Chem Soc (105): 1407–1413.